Advances in Water Resources 111 (2018) 372–380

Contents lists available at ScienceDirect

Advances in Water Resources

journal homepage: www.elsevier.com/locate/advwatres

Characterizing the impact of model error in hydrologic time series recovery inverse problems

Scott K. Hansen*,[a], Jiachuan He[a,b], Velimir V. Vesselinov[a]

[a] Computational Earth Science Group (EES-16), Los Alamos National Laboratory, USA
[b] Computational Hydraulics Group (CHG), Institute for Computational Engineering and Sciences (ICES), The University of Texas at Austin, USA

ABSTRACT

Hydrologic models are commonly over-smoothed relative to reality, owing to computational limitations and to the difficulty of obtaining accurate high-resolution information. When used in an inversion context, such models may introduce systematic biases which cannot be encapsulated by an unbiased "observation noise" term of the type assumed by standard regularization theory and typical Bayesian formulations. Despite its importance, model error is difficult to encapsulate systematically and is often neglected. Here, model error is considered for an important class of inverse problems that includes interpretation of hydraulic transients and contaminant source history inference: reconstruction of a time series that has been convolved against a transfer function (i.e., impulse response) that is only approximately known. Using established harmonic theory along with two results established here regarding triangular Toeplitz matrices, upper and lower error bounds are derived for the effect of model error on time series recovery for both well-determined and over-determined inverse problems. It is seen that use of additional measurement locations does not improve expected performance in the face of model error. A Monte Carlo study of a realistic hydraulic reconstruction problem is presented, and the lower error bound is seen informative about expected behavior. A possible diagnostic criterion for blind transfer function characterization is also uncovered.

1. Introduction

Inverse analyses now form a major part of research in hydrology, being relevant to hydraulic tomography, contaminant source identification, and model parametrization. In the inverse problems literature, it is common to assume a perfect model, with all divergence between model prediction and the observed data vector attributable to "noise" drawn from a symmetric, zero-mean probability distribution function. This theoretical approach underlies classical regularization methods such as Tikhonov and TSVD techniques (Hansen, 1992), and is also typically used for specifying the likelihood function in the Bayesian inversion paradigm (Bui-Thanh, 2012). That the approach of encoding all errors as unbiased measurement uncertainties may not be appropriate in hydrologic inverse modeling has been recognized. However in the absence of a paradigm that captures model error in a systematic fashion, the perfect-model assumption remains common in practice (Del Giudice et al., 2015; Lin and Beck, 2012).

The effect of model error has received some attention in recent hydrological literature. Following the categorization of model error research by Montanari (2007) into studies of (i) forward modeling, and (ii) model calibration, selection, and input signal recovery, we note more recent research appears to have been devoted to the former (e.g., Gupta et al., 2008; Vrugt et al., 2008; Lin and Beck, 2012; Gong et al., 2013; Vrugt and Sadegh, 2013; White et al., 2014), with some attention also devoted to its effect on model selection and parametrization (e.g. Gaganis and Smith, 2001; Doherty and Welter, 2010). Systematic, qualitative treatments of the problem of model error have been presented by Refsgaard et al. (2006) and by Gupta et al. (2012).

Current approaches to quantifying the effect of model error are typically probabilistic, treating the impact of the model uncertainty on output with Bayesian (Krzysztofowicz, 1999) or information theoretic (Gong et al., 2013) formalisms. The uncertainty about model structure is commonly modeled by parameterizing the model itself as a probability distribution function (pdf) linking inputs and outputs, or as a deterministic numerical model with pdfs defined on its state variables (see summary in Renard et al., 2010). A number of conceptual approaches for treating model error in a theoretical framework have appeared in the literature. A popular approach, originating with Kennedy and O'Hagan (2001), works in a Bayesian framework and treats model error as a Gaussian process whose governing parameters

* Corresponding author.
E-mail address: skh3@lanl.gov (S.K. Hansen).

http://dx.doi.org/10.1016/j.advwatres.2017.09.030
Received 24 February 2017; Received in revised form 22 September 2017; Accepted 23 September 2017
Available online 28 October 2017
0309-1708/ Published by Elsevier Ltd.

must be recovered alongside model parameters during the calibration process. The original work was focused upon prediction, but Brynjarsdóttir and O'Hagan (2014) have recently investigated the approach specifically in the context of parametric inference. This approach has also been generalized and applied in a water resources context by Xu and Valocchi (2015). Bayesian approaches to model selection may also specifically account for model error through the selection of their likelihood term. This is done explicitly in the GLUE approach of Beven and Binley (1992), in which the likelihood function is selected subjectively with an eye to capturing model error. An alternative Bayesian model selection approach is proposed by Gaganis and Smith (2001). They propose a scheme in which the likelihood function has a uniform distribution inside a hypercube centered around the observation vector, whose volume represents tolerable error. Data is increasingly added to the calibration, until the probability of all but one model (which is selected) decreases. By decreasing the volume of the hypercube until the probability of the selected model decreases, a measure of the misfit attributable to model error is derived. This approach, similar to the BIC (Schwarz, 1978) and KIC (Kashyap, 1982) model selection criteria, assumes that the true likelihood function is sharply peaked around the maximum likelihood parameters. Finally, we note the approach of Doherty and Welter (2010), White et al. (2014), and collaborators, which is to focus on linear models and their coarse-graining into lower-dimensional subset models. Employing the singular value decomposition and other techniques of matrix analysis, these authors consider the impact of dimensionality reduction on parametrization, and on the accuracy of prediction.

An alternative to symbolic treatment of model error is to explore its effects numerically, using a Monte Carlo study. The approximate Bayesian computation approach of Vrugt and Sadegh (2013) also uses a box likelihood function similar to that of Gaganis and Smith (2001) along with a Markov-chain Monte Carlo approach: all predictions which generate output sufficiently close to the observation data are considered samples from the posterior distribution. Another Monte Carlo approach, due to Hansen and Vesselinov (2016), determines probability distributions for inferred parameters by generating an ensemble of data with a superset model and then interpreting it with the model of interest.

The current paper follows the path of treating models (and model error) symbolically, but differs from the schemes mentioned above. Rather than treating models as Gaussian processes or arbitrary probability distributions, they are treated as generalized Fourier series with imperfectly known coefficients. The focus here is on a specific class of inverse problems commonly faced by hydrologists: time series recovery problems with a temporal convolution structure. More concretely, this means the recovery of an input signal from one or more remote output signal measurements, where each output signal is generated by temporal convolution of the shared input signal with a unique transfer function, which is only approximately known. Intuitively: the output behavior at each observation location is defined by the response at the same location to an instantaneous pulse at a remote location, and superposition in time may be used to determine the output resulting from an arbitrary transient input signal at the same input location.

Expressed symbolically, we consider problems in which we wish to recover a transient input signal at location $\boldsymbol{0}$, $h(\boldsymbol{0}, t)$, which has caused a transient output signal, $h(\boldsymbol{x}, t)$, at a remote location $\boldsymbol{x}$, by means of the convolution

$$h(\boldsymbol{x}, t) = b(\boldsymbol{x}, t)*h(\boldsymbol{0}, t) = \int_0^t b(\boldsymbol{x}, t-\tau)h(\boldsymbol{0}, \tau)d\tau. \tag{1}$$

Here, $b(\boldsymbol{x}, t)$ is a Green's function (i.e., transfer function) representing the response to an instantaneous Dirac input signal at the origin (i.e. $h(\boldsymbol{0}, t) = \delta(t)$). The convolution in Eq. (1) describes to a wide range of problems, and applies to essentially any transient system that is governed by a linear (integro-)differential equation, such as the groundwater flow equation or the advection-dispersion equation. Only linearity in the dependent variable is required for this structure to describe the physics: dependence on parameters such as hydraulic conductivity may be nonlinear and these parameters may be spatially heterogeneous. Examples of hydrologic inverse problems that may be expressed in this form include the inference of hydraulic head history at some location of interest from available time series obtained at remote monitoring wells, and the inference of the contaminant source history at a given location from remotely-obtained breakthrough curves. In both of these examples, the transfer function is the same as the impulse response—the response to an instantaneous pulse of concentration or head.

We quantify error with the metric ϵ, defined as the squared L^2 norm of the error of the inferred input signal, $\tilde{h}(\boldsymbol{0}, t)$, relative to the true signal, $h(\boldsymbol{0}, t)$. This is defined mathematically as

$$\epsilon \equiv \int_0^\infty (h(\boldsymbol{0}, t) - \tilde{h}(\boldsymbol{0}, t))^2 dt. \tag{2}$$

We are primarily interested in how ϵ is affected by error in the assumed transfer function used in inversion relative to the true transfer function which perfectly generates the observed output signal, although we shall make other observations.

For inverse problems of the sort described by Eq. (1), it is shown in Section 2 how it is possible to formally decompose the transfer function(s) as well as the input and output signals into generalized Fourier series. Some apparently new results concerning triangular Toeplitz matrices are established (in Appendix A), and techniques of matrix analysis are then employed to derive concrete bounds on the signal reconstruction error as a function of the error in dominant components of the transfer function(s). In Section 3, a Monte Carlo study of hydraulic inversion is presented which contextualizes the theoretical results shown in Section 2 and some empirical observations that go beyond the theoretical work are noted. Section 4 summarizes what has been learned and suggests interesting future research directions.

2. Derivation of error bounds

2.1. Laguerre expansion method

In general, for some fixed $\boldsymbol{x}$, the input signal, transfer function, and output signal can be expanded as generalized Fourier series in a basis of Laguerre functions, $\phi_n(\cdot)$ ($n \geq 0$). Each Laguerre function is defined according to the formula:

$$\phi_n(t) = \frac{e^{\frac{t}{2}}}{n!}\frac{d^n}{dt^n}(e^{-t}t^n), \tag{3}$$

and together they form an orthonormal basis on $[0, \infty)$ (Abate et al., 1996). This means that any well-behaved function defined on $[0, \infty)$ can be expressed as an infinite series of Laguerre functions and approximated by a finite series. The significance from our point of view is that arbitrary functions can be expressed as finite-length vectors (containing the coefficient of each function in the finite-length Laguerre series expansion). We write the Laguerre series expansions for, respectively, the input signal, a transfer function, and an output signal in Eq. (1) as follows:

$$h(\boldsymbol{0}, t) = \sum_n a_n \phi_n\left(\frac{t}{T}\right), \tag{4}$$

$$b(\boldsymbol{x}, t) = \sum_n b_n \phi_n\left(\frac{t}{T}\right), \tag{5}$$

$$h(\boldsymbol{x}, t) = \sum_n c_n \phi_n\left(\frac{t}{T}\right). \tag{6}$$

Here, T is a characteristic time of the problem, chosen to accelerate

convergence of the infinite series (regardless of the choice of T, the infinite series converge). Let $\mathbf{c}$ be a vector of N Laguerre coefficients, such that its n-th entry, $\mathbf{c}_n = c_n$. Similarly, define $\mathbf{a}$ to be a vector of N Laguerre coefficients, such that $\mathbf{a}_n = a_n$. It has been shown (Hansen and Kueper, 2009) that, in general, these vectors of coefficients can be related by the matrix operation

$$\mathbf{c} = \mathbf{B}\mathbf{a}, \tag{7}$$

where $\mathbf{B}$ is the following lower triangular Toeplitz (LTT) matrix:

$$\mathbf{B} = T\begin{bmatrix} b_0 & 0 & 0 & \cdots & 0 \\ b_1 - b_0 & b_0 & 0 & \cdots & 0 \\ b_2 - b_1 & b_1 - b_0 & b_0 & \cdots & 0 \\ \vdots & \vdots & \vdots & \ddots & \vdots \\ b_{N-1} - b_{N-2} & b_{N-2} - b_{N-3} & b_{N-3} - b_{N-4} & \cdots & b_0 \end{bmatrix}. \tag{8}$$

We have now converted the convolution inverse problem into a matrix inverse problem, involving a matrix with a large amount of structure; we will employ this structure to place bounds on the inversion error of the original convolution problem. Because $\mathbf{B}$ is a full-rank square matrix, if it is known perfectly then inversion is well defined (although not necessarily numerically stable):

$$\mathbf{B}^{-1}\mathbf{c} = \mathbf{a}. \tag{9}$$

To continue the analysis of the this section, we need to establish two properties of LTT matrices, which may not be of interest to practically-oriented readers. This analysis is presented in Appendix A.

2.2. Effect of imperfect model: single observation location

We now consider the core problem, the impact of model error on signal inference, in the simplest case: that of a single output signal. Assume perfect knowledge of output signal $h(\boldsymbol{x}, t)$, but imperfect knowledge of transfer function $b(\boldsymbol{x}, t)$, and a need to infer input signal $h(\boldsymbol{0}, t)$. The imperfect knowledge of b will lead to an approximate solution for the input signal, $\tilde{h}(\boldsymbol{0}, t)$, whose Laguerre coefficients, $\tilde{a}_n$, lie in vector $\tilde{\mathbf{a}}$. In matrix form, this can be written by distinguishing the (unknown) true matrix, $\mathbf{B}$, from the approximate matrix, $\widetilde{\mathbf{B}}$, resulting from our imperfect knowledge of b. The matrix inverse problem that is being solved is thus

$$\mathbf{c} = \widetilde{\mathbf{B}}\tilde{\mathbf{a}}. \tag{10}$$

Parseval's equation (Churchill, 1963, p. 61) states that if a function, $f(t)$, has a representation in orthogonal basis functions, $\psi_n(t)$, on an interval (α, β), such that $f(t) = \sum_n q_n \phi_n(t)$, then it is true that $\int_\alpha^\beta (f(t))^2 dt = \sum_n q_n^2$. By making the definition $f(t) = h(\boldsymbol{0}, t) - \tilde{h}(\boldsymbol{0}, t)$, it follows that $q_n = a_n - \tilde{a}_n$, and we immediately are able to express the squared error of our source history estimate in vector form, using Eq. (2), as

$$\epsilon = \int_0^\infty (h(\boldsymbol{0}, t) - \tilde{h}(\boldsymbol{0}, t))^2 dt \approx \|\mathbf{a} - \tilde{\mathbf{a}}\|_2^2, \tag{11}$$

with equality in the limit $N \to \infty$. Although the error introduced by *spectral leakage* (i.e., series truncation) has been recognized as important in some geophysical inversion (Sneider and Trampert, 1999), many transfer functions and input signals are smooth in hydrology, and the approximate equality will be taken to be exact in subsequent analysis. The error analysis can thus be performed in the matrix domain.

Because $\widetilde{\mathbf{B}}$ and $\mathbf{B}$ are invertible, there is a unique solution to Eq. (10) and thus:

$$\|\mathbf{a} - \tilde{\mathbf{a}}\|_2 = \|(\mathbf{I} - \widetilde{\mathbf{B}}^{-1}\mathbf{B})\mathbf{a}\|_2. \tag{12}$$

Because $\mathbf{I}$, $\widetilde{\mathbf{B}}$, and $\mathbf{B}$ are LTT, it follows from application of Lemma 1 and Lemma 2 (see Appendix A) that $\mathbf{I} - \widetilde{\mathbf{B}}^{-1}\mathbf{B}$ is an LTT matrix. Let $\widetilde{\mathbf{b}}^{-1}$, $\mathbf{b}$, and $\mathbf{e}$ be the vectors of coefficients on the diagonals and sub-diagonals of the LTT matrices $\widetilde{\mathbf{B}}^{-1}$, $\mathbf{B}$, and $\mathbf{I} - \widetilde{\mathbf{B}}^{-1}\mathbf{B}$, respectively, indexed as in the proof of Lemma 2. For clarity, we mean that $\mathbf{b}_0$ equals the identical elements on the diagonal of $\mathbf{B}$, $\mathbf{b}_1$ equals the identical elements on the first sub-diagonal of $\mathbf{B}$, and so on. From inspection of Eq. (8), $\mathbf{b}_0 = b_0$ and $\mathbf{b}_1 = b_1 - b_0$. By applying Eq. (A.1) with A defined as the upper right 2×2 sub-matrix of $\widetilde{\mathbf{B}}$, it follows immediately that $\widetilde{\mathbf{b}}^{-1}{}_0 = \frac{1}{\tilde{b}_0}$ and $\widetilde{\mathbf{b}}^{-1}{}_1 = -\frac{\tilde{b}_1 - \tilde{b}_0}{\tilde{b}_0^2}$. We may then apply Eq. (A.5) to determine the diagonal and sub-diagonal elements of the LTT matrix $\widetilde{\mathbf{B}}^{-1}\mathbf{B}$. It is then trivial to determine the elements of the LTT matrix $\mathbf{I} - \widetilde{\mathbf{B}}^{-1}\mathbf{B}$, whose elements are contained in vector $\mathbf{e}$. In particular,

$$\mathbf{e}_0 = 1 - \frac{b_0}{\tilde{b}_0} \tag{13}$$

$$\mathbf{e}_1 = \frac{1}{\tilde{b}_0}\left[b_1 - \tilde{b}_1\left(\frac{b_0}{\tilde{b}_0}\right)\right]. \tag{14}$$

Note that these elements (like all of $\mathbf{e}$) are zero when $\widetilde{\mathbf{B}} = \mathbf{B}$.

The following lower error bound follows from consideration of the first element of $(\mathbf{I} - \widetilde{\mathbf{B}}^{-1}\mathbf{B})\mathbf{a}$:

$$\boxed{\left|a_0\right|\left|1 - \frac{b_0}{\tilde{b}_0}\right| \le \|\mathbf{a} - \tilde{\mathbf{a}}\|_2,} \tag{15}$$

In the useful special case in which the input signal is an arbitrary decaying exponential (with rate constant $1/2T$, noting that T is a free parameter), the only nonzero term of its Laguerre series is a_0 and a lower bound on the *relative* error follows immediately:

$$\boxed{\left|1 - \frac{b_0}{\tilde{b}_0}\right| \le \frac{\|\mathbf{a} - \tilde{\mathbf{a}}\|_2}{\|\mathbf{a}\|_2}.} \tag{16}$$

The significance of these results is that we are able to bound the L^2 error of the reconstruction of $h(\boldsymbol{0}, t)$ (essentially the squared error, integrated over time) using only the most significant components of the Laguerre expansions of the true transfer function, $b(\boldsymbol{0}, t)$ and the approximately known transfer function $\tilde{b}(\boldsymbol{0}, t)$. We may have some prior knowledge of possible transfer function shapes and to be able to qualify this quantity despite not having exact knowledge of the true transfer function.

The coefficient b_0 is computed

$$b_0 = \int_0^\infty e^{-\frac{t}{2}} b(0, t) dt, \tag{17}$$

and similarly for $\tilde{b}_0$. It should be clear that if $b(\boldsymbol{x}, t)$ and $\tilde{b}(x, t)$ have different shapes (particularly if $\tilde{b}(x, t)$ represents transmission through a homogeneous medium, and the true Green's function, $b(\boldsymbol{x}, t)$, characterizes a medium that is heterogeneous or homogeneous with substantially different properties) then it is possible to have $b_0/\tilde{b}_0 \gg 1$. In such cases, the error due to fitting of the inaccurate model overwhelms the signal and the errors of signal measurement (detection).

It is generally possible to use the approach developed here to generate lower error bounds relating the first k terms of the sequences $\{a_n\}$, $\{b_n\}$, and $\{\tilde{b}_n\}$, for arbitrary k, depending on the amount of information available about the transfer function. For instance, for $k = 2$:

$$\left|a_0\left(1 - \frac{b_0}{\tilde{b}_0}\right)\right|^2 + \left|a_0\left(\frac{1}{\tilde{b}_0}\left[b_1 - \tilde{b}_1\left(\frac{b_0}{\tilde{b}_0}\right)\right]\right) + a_1\left(1 - \frac{b_0}{\tilde{b}_0}\right)\right|^2 \le \|\mathbf{a} - \tilde{\mathbf{a}}\|_2^2. \tag{18}$$

It is also possible to derive an upper bound, which does not depend on $\{a_n\}$, but which requires $k = N$ terms of the other sequences. This is seen in the next section.

2.3. Effect of imperfect model: multiple observation locations

In the case of M monitoring locations, the problem is generally overdetermined, and instead of directly computing the inverse, one may define the optimal solution, $\tilde{\mathbf{a}}$, as the one which minimizes the sum of

squared residuals at each observation location, i.e., satisfies the following condition:

$$\sum_{l=1}^{M}\left\|\mathbf{c_l}-\widetilde{\mathbf{c}}_\mathbf{l}\right\|_2^2=\min_{\tilde{\mathbf{a}}}\sum_{l=1}^{M}\|\mathbf{c_l}-\widetilde{\mathbf{c}}_\mathbf{l}\|_2^2. \tag{19}$$

This problem may be placed in a matrix form by defining the block diagonal matrices

$$\mathbf{B}_\otimes=\begin{bmatrix}\mathbf{B_1} & 0 & \cdots & 0\\ 0 & \mathbf{B_2} & \cdots & 0\\ \vdots & \vdots & \ddots & \vdots\\ 0 & 0 & \cdots & \mathbf{B_M}\end{bmatrix}, \tag{20}$$

$$\widetilde{\mathbf{B}}_\otimes=\begin{bmatrix}\widetilde{\mathbf{B}}_\mathbf{1} & 0 & \cdots & 0\\ 0 & \widetilde{\mathbf{B}}_\mathbf{2} & \cdots & 0\\ \vdots & \vdots & \ddots & \vdots\\ 0 & 0 & \cdots & \widetilde{\mathbf{B}}_\mathbf{M}\end{bmatrix}. \tag{21}$$

It is also useful to define the following block-columnar matrix of M, $N \times N$ identity matrices:

$$\mathbf{D}=\begin{bmatrix}\mathbf{I_N}\\ \mathbf{I_N}\\ \vdots\\ \mathbf{I_N}\end{bmatrix}. \tag{22}$$

Using this notation, and recalling that for any vector $\mathbf{v}$, $\|\mathbf{v}\|_2^2=\mathbf{v^Tv}$, the LHS of Eq. (19) can be represented as:

$$\sum_{l=1}^{M}\|\mathbf{c_l}-\widetilde{\mathbf{c}}_\mathbf{l}\|_2^2=\mathbf{a^TD^TB_\otimes^TB_\otimes Da}-2\mathbf{a^TD^TB_\otimes^T\widetilde{B}_\otimes\tilde{a}}+\tilde{\mathbf{a}}^\mathbf{T}\mathbf{D^T\widetilde{B}_\otimes^T\widetilde{B}_\otimes D\tilde{a}}. \tag{23}$$

By definition, $\tilde{\boldsymbol{\alpha}}$, must minimize this quantity, implying that it is at a location where the vector derivative of the RHS of Eq. (23) with respect to $\tilde{\boldsymbol{\alpha}}$ is zero. Differentiating,

$$\frac{d}{d\tilde{\mathbf{a}}}\sum_{l=1}^{M}\|\mathbf{c_l}-\widetilde{\mathbf{c}}_\mathbf{l}\|_2^2=\frac{d}{d\tilde{\mathbf{a}}}[-2\mathbf{a^TD^TB_\otimes^T\widetilde{B}_\otimes\tilde{a}}+\tilde{\mathbf{a}}^\mathbf{T}\mathbf{D^T\widetilde{B}_\otimes^T\widetilde{B}_\otimes D\tilde{a}}] \tag{24}$$

$$=-2\mathbf{a^TD^TB_\otimes^T\widetilde{B}_\otimes D}+2\tilde{\mathbf{a}}^\mathbf{T}\mathbf{D^T\widetilde{B}_\otimes^T\widetilde{B}_\otimes D} \tag{25}$$

The optimal solution will be when this quantity equals zero, which may be seen by inspection to be satisfied when

$$\mathbf{D\tilde{a}}=\widetilde{\mathbf{B}}_\otimes^{-1}\mathbf{B}_\otimes\mathbf{Da}, \tag{26}$$

and this will be the only solution in the general case of full rank $\widetilde{\mathbf{B}}_\otimes\mathbf{D}$. Because $\mathbf{D^TD}=M\,\mathbf{I_N}$, we arrive at the solution

$$\tilde{\mathbf{a}}=\frac{1}{M}\mathbf{D^T}\widetilde{\mathbf{B}}_\otimes^{-1}\mathbf{B}_\otimes\mathbf{Da}. \tag{27}$$

It follows from the definition of $\mathbf{D}$ that

$$\|\mathbf{a}-\tilde{\mathbf{a}}\|_2=\frac{1}{M}\|\mathbf{Da}-\mathbf{D\tilde{a}}\|_2, \tag{28}$$

from which it follows from Eq. (26) that

$$\|\mathbf{a}-\tilde{\mathbf{a}}\|_2=\frac{1}{M}\|(\mathbf{I_{MN}}-\widetilde{\mathbf{B}}_\otimes^{-1}\mathbf{B}_\otimes)\mathbf{Da}\|_2. \tag{29}$$

This is of a superficially similar form to Eq. (12), however the matrices $\widetilde{\mathbf{B}}_\otimes$ and $\mathbf{B}_\otimes$ are merely triangular, but not LTT, and so Eq. (29) cannot be analyzed in the same way. Nevertheless, by inspection and use of the rules for matrix block multiplication, it is apparent that

$$\|\mathbf{a}-\tilde{\mathbf{a}}\|_2=\frac{1}{M}\sum_{l=1}^{M}\|(\mathbf{I_N}-\widetilde{\mathbf{B}}_\mathbf{l}^{-1}\mathbf{B_l})\mathbf{a}\|_2. \tag{30}$$

This is simply the average of the individual model errors if only a single monitoring location were to be used (see Eq. (12)), implying that the lower error bound theory developed above can be carried over straightforwardly. If $\mathbf{a}$ is viewed as a random variable, *the expected error is also not reduced by incorporating additional measurements, unlike the scenario of uncorrelated random noise*.

One can also derive an upper bound on the relative error of $\tilde{\mathbf{a}}$ from Eq. (29) using the definition of the induced matrix 2-norm $\|\cdot\|_2$, the fact it is always less than or equal to the Frobenius norm, and the fact that $\frac{1}{M}\|\mathbf{Da}\|_2=\|\mathbf{a}\|_2$. From this, it follows that

$$\boxed{\frac{\|\mathbf{a}-\tilde{\mathbf{a}}\|_2}{\|\mathbf{a}\|_2}\le\|\mathbf{I_{MN}}-\widetilde{\mathbf{B}}_\otimes^{-1}\mathbf{B}_\otimes\|_2\le\|\mathbf{I_{MN}}-\widetilde{\mathbf{B}}_\otimes^{-1}\mathbf{B}_\otimes\|_F,} \tag{31}$$

where $\|\cdot\|_F$ represents the Frobenius norm. Practically, this depends on the full sets of coefficients $\{b_n\}$ and $\{\tilde{b}_n\}$, which is a greater information demand than for the lower bounds, which only involve relationships of the dominant components.

Naturally, Eq. (31) applies to single measurement location reconstruction as a special case. In this case, the Frobenius norm can be computed symbolically using the entries in $\mathbf{e}$, and it may be possible to derive an estimate of the upper bound in terms of only dominant components, as in the case of the lower bound.

3. Monte Carlo study: reconstruction of hydraulic transients

In this section, the inference of a hydraulic head transient history along an aquifer boundary (which might be interpreted as a river stage transient, where the river is in a hydraulic connection with the aquifer) based on a time series of measurements made at a single nearby groundwater monitoring well is considered. This study represents a demonstration of the ideas developed above, and also may be of independent interest.

An ensemble of hydraulic transients, $\{h_i(\boldsymbol{x}, t)\}$, "observed" at a fixed $\boldsymbol{x}$ are considered. These are all generated by convolving a single input transient, $h(\mathbf{0}, t)$, with a number of equally-likely transfer functions corresponding to complex groundwater models, $\{b_i(\boldsymbol{x}, t)\}$. Each of these "true" groundwater models may be equally well represented by the same simplified interpretive groundwater model, which corresponds to the transfer function $\tilde{b}(\boldsymbol{x}, t)$. We invert the ensemble of output signals using $\tilde{b}(\boldsymbol{x}, t)$ to generate an ensemble of reconstructed input signals, $\{\tilde{h}_i(\mathbf{0}, t)\}$, and examine the reconstruction error, ϵ. Note that rather than considering a variety of interpretive models and a single true model, as in a traditional model calibration exercise, we are here considering the converse situation.

3.1. Procedure

It is assumed here that the specific storage is known and spatially uniform, and that the log hydraulic conductivity is defined by a multi-Gaussian spatially random field whose mean is known, but which is otherwise unknown. Assuming flow is described by the groundwater flow equation on this heterogeneous conductivity field, $b(\boldsymbol{x}, t)$ is the head history at a fixed location, $\boldsymbol{x}$. A natural interpretive model is selected: the same groundwater flow equation, but solved on a homogeneous conductivity field that is everywhere equal to the mean of the true log hydraulic conductivity field.

The study is then performed according to the following basic procedure: First, a true, exponentially decaying, transient in the river stage on the aquifer domain boundary is specified, along with the location of a monitoring well at which a time series of head measurements is to be made. The accuracy of reconstruction of the river stage transient from the transient at the monitoring well is studied, given an overly smooth model of the subsurface. For simplicity, the free parameter, T, is selected so that the Laguerre decomposition of the true transient using Eq. (4) yields the vector $\mathbf{a}$ = <1, 0, 0, ⋯,0>. Next, 500 two-dimensional subsurface realizations are generated with different heterogeneous log-hydraulic conductivity fields, all of which have the same multi-

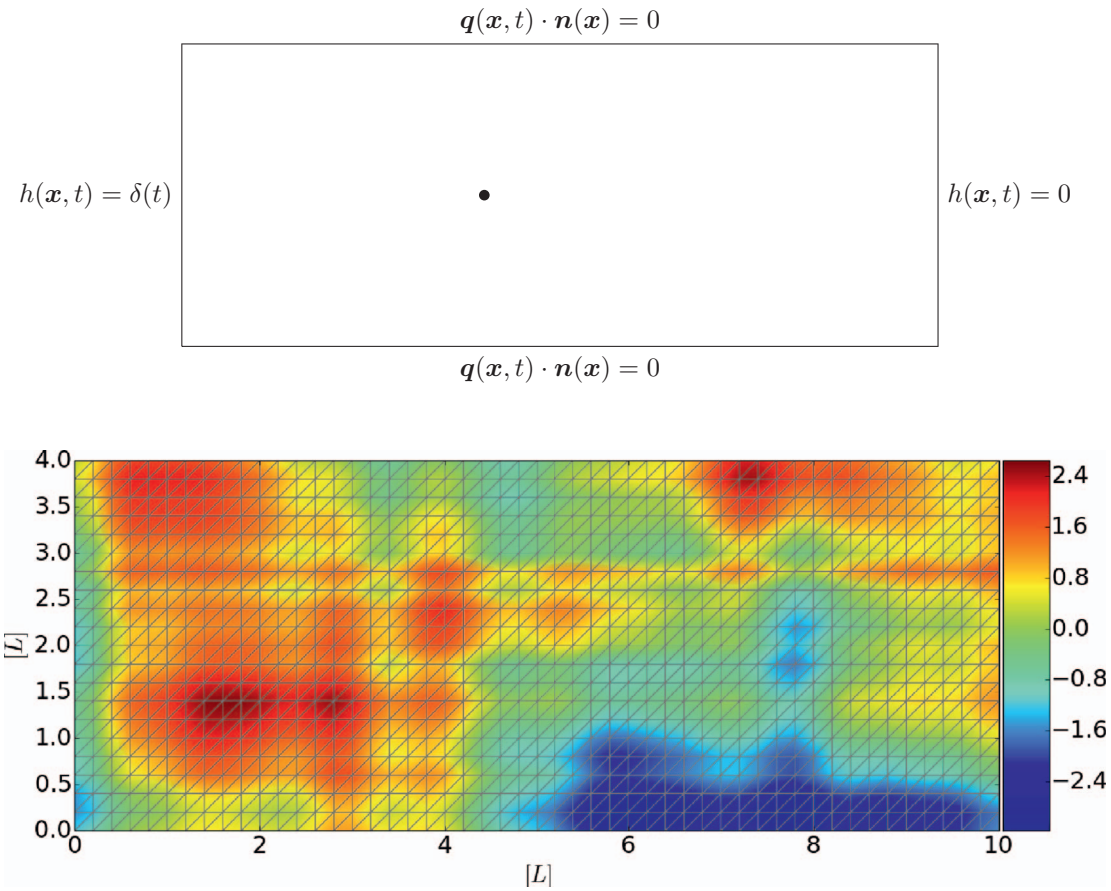

Fig. 1. Top: the flow domain and the observation location (black dot). Bottom: example of a realization of ln [$K(\boldsymbol{x})$] field along with the mesh used to numerically solve Eq. (37).

Gaussian statistical correlation structure and geometric mean conductivity. Subsequently, using finite element analysis, head time series are computed at the monitoring well for each of the 500 subsurface realizations resulting from a Dirac head impulse at the river stage. Each impulse response (Green's function) is decomposed as a vector of Laguerre coefficients, $\mathbf{b}$. Again, using finite element analysis, the impulse response at the well is computed, but assuming a uniform hydraulic conductivity field with the same geometric mean hydraulic conductivity as used in each of the heterogeneous realizations. This impulse response is decomposed as a vector of Laguerre coefficients, $\widetilde{\mathbf{b}}$. Finally, for each realization, the reconstruction error, $\|(\mathbf{I}-\widetilde{\mathbf{B}}^{-1}\mathbf{B})\mathbf{a}\|_2$, is computed and compared with the analytical lower bound in Eq. (16). Statistics about this quantity are tabulated so that its relationship to qualitative features of the inverse model discrepancy may be studied.

Both the true solution and the interpretive model are described by the following system of equations:

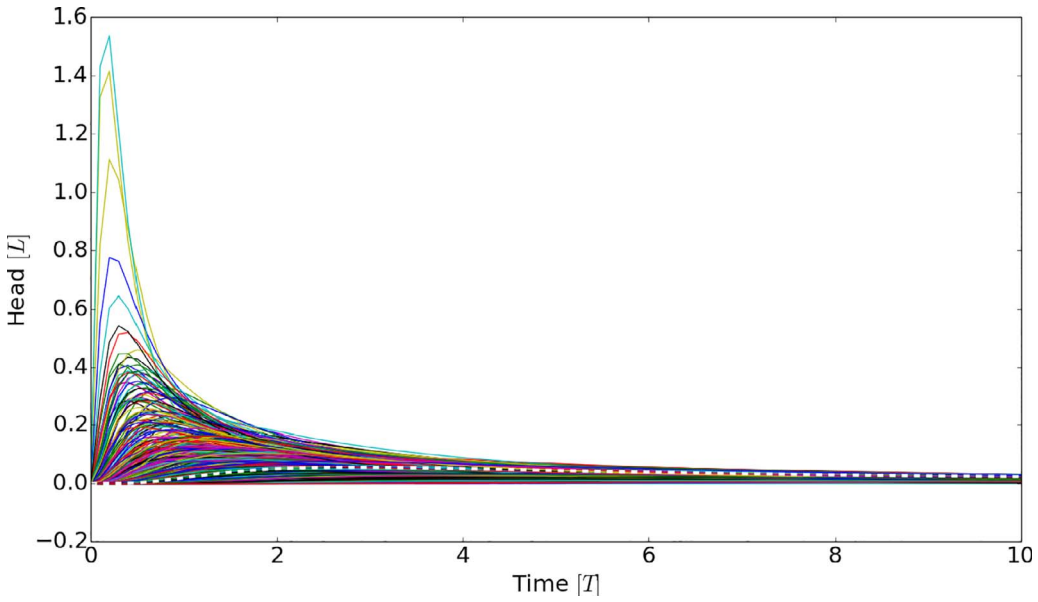

Fig. 2. Hydraulic head transient responses at the point $(x, y) = (4, 2)$ due to an impulse at the boundary $x = 0$. Impulse responses—i.e., $b(4, 2, t)$—for 500 random realizations of the hydraulic conductivity field are shown (solid, colored lines), along with the response from the interpretation model—i.e., $\tilde{b}(4, 2, t)$—with spatially uniform hydraulic conductivity, $K(\boldsymbol{x}) = 1\ [LT^{-1}]$ (dashed, white line).

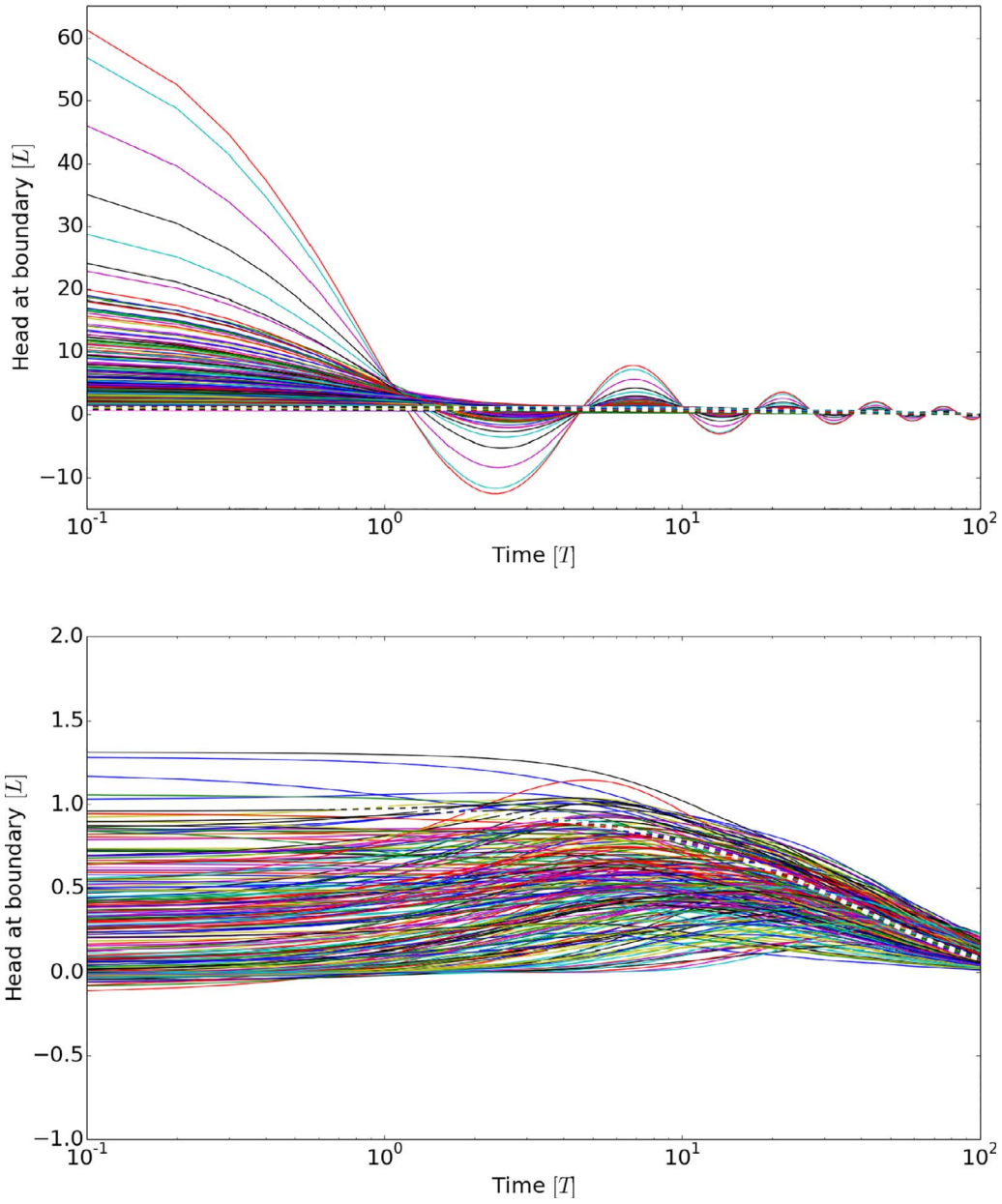

Fig. 3. Reconstructions of the boundary condition resulting from application of the interpretation model to output from the 500 simulations performed in heterogeneous aquifers (colored lines) along with the actual boundary condition used in the simulations (dashed white line). Responses are partitioned according to whether true peak hydraulic head is earlier (top axes) than assumed by the interpretive model, or later (bottom axes).

$$S_s \frac{\partial h(\boldsymbol{x}, t)}{\partial t} + \nabla \cdot \boldsymbol{q}(\boldsymbol{x}, t) = 0, \quad \boldsymbol{x} \in \boldsymbol{D} \tag{32}$$

$$\boldsymbol{q}(\boldsymbol{x}, t) = -K(\boldsymbol{x}) \nabla h(\boldsymbol{x}, t), \quad \boldsymbol{x} \in \boldsymbol{D} \tag{33}$$

solved subject to the initial and boundary conditions

$$h(\boldsymbol{x}, 0) = 0, \quad \boldsymbol{x} \in \boldsymbol{D} \tag{34}$$

$$h(\boldsymbol{x}, t) = c(t), \quad \boldsymbol{x} \in \Gamma_L \tag{35}$$

$$h(\boldsymbol{x}, t) = 0, \quad \boldsymbol{x} \in \Gamma_R \tag{36}$$

$$\boldsymbol{q}(\boldsymbol{x}, t) \cdot \boldsymbol{n}(\boldsymbol{x}) = 0, \quad \boldsymbol{x} \in \Gamma_S \tag{37}$$

where the only difference enters due to different choices for $K(\boldsymbol{x})$. In the above equations, $\boldsymbol{x}$ [L] represents the location, t [T] represents time, S_s [L^{-1}] represents specific storage, h [L] represents hydraulic head, $\boldsymbol{q}$ [LT^{-1}] represents groundwater flux, K [LT^{-1}] represents hydraulic conductivity, and $\boldsymbol{n}$ [1] is the outward-facing unit normal vector. For vector quantities, the units reported are for each of their components.

More concretely, a two-dimensional model of saturated flow in a heterogeneous porous medium is defined over the rectangular domain $\boldsymbol{D} = (0, L_1) \times (0, L_2)$, where $L_1 = 10$ [L] and $L_2 = 4$ [L] (L is any consistent length unit), and specific storage, $S_s = 1$ (Fig. 1). Γ_L represents the left boundary of $\boldsymbol{D}$ (at $x = 0$), Γ_R represents the right boundary of $\boldsymbol{D}$ (at $x = 10$), and Γ_S represents the union of the other two sides of $\boldsymbol{D}$ (at $y = 0$ and $y = 4$, respectively). Let $Y(\boldsymbol{x}, \omega) = \ln[K(\boldsymbol{x}, \omega)]$ be a random field, where ω belongs to the space of random events $\boldsymbol{\Omega}$. Assuming $Y(\boldsymbol{x}, \omega)$ is Gaussian with zero mean and a separable exponential covariance function,

$$C(\boldsymbol{x_1}, \boldsymbol{x_2}) = C(x_1, y_1; x_2, y_2) = \sigma_Y^2 \exp\left[-\frac{|x_1 - x_2|}{\eta_1} - \frac{|y_1 - y_2|}{\eta_2}\right], \tag{38}$$

where $\sigma_Y^2 = 2$, $\eta_1 = 4$ and $\eta_2 = 2$ are the variance and the correlation lengths of the random field.

For the Monte Carlo study, a set of 500 realizations of $b(t)$ is generated by setting $c(t) = \delta(t)$, generating 500 $\ln[K(\boldsymbol{x})]$ fields Fig. 1, bottom), using a 100-term truncated Karhunen-Loève expansions (KLE) to represent the field as weighted sums of predefined spatially variable orthonormal functions (Zhang and Lu, 2004), and solving Eqs. (32–37) on each. The

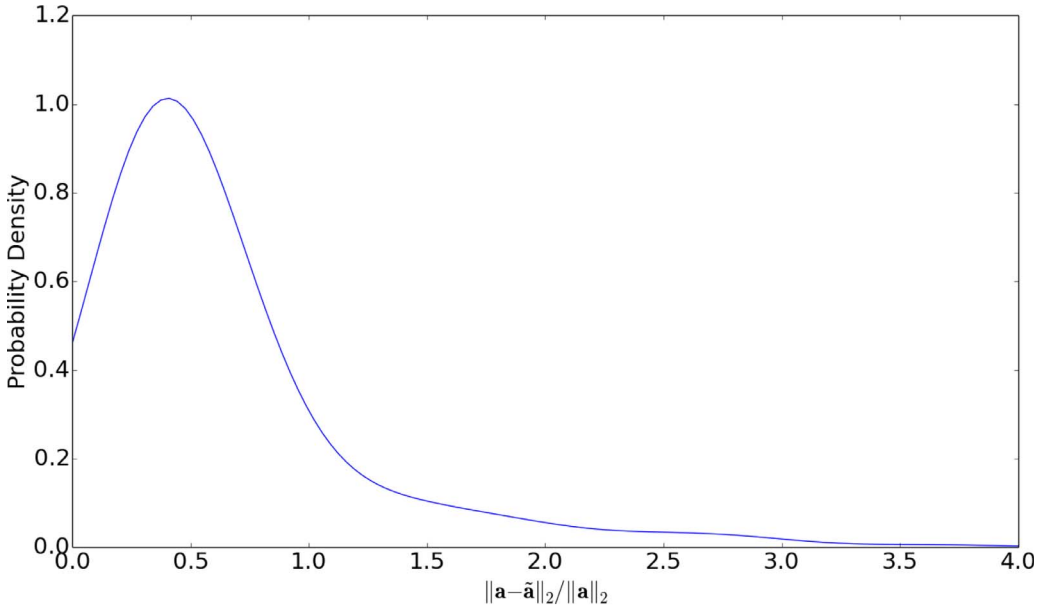

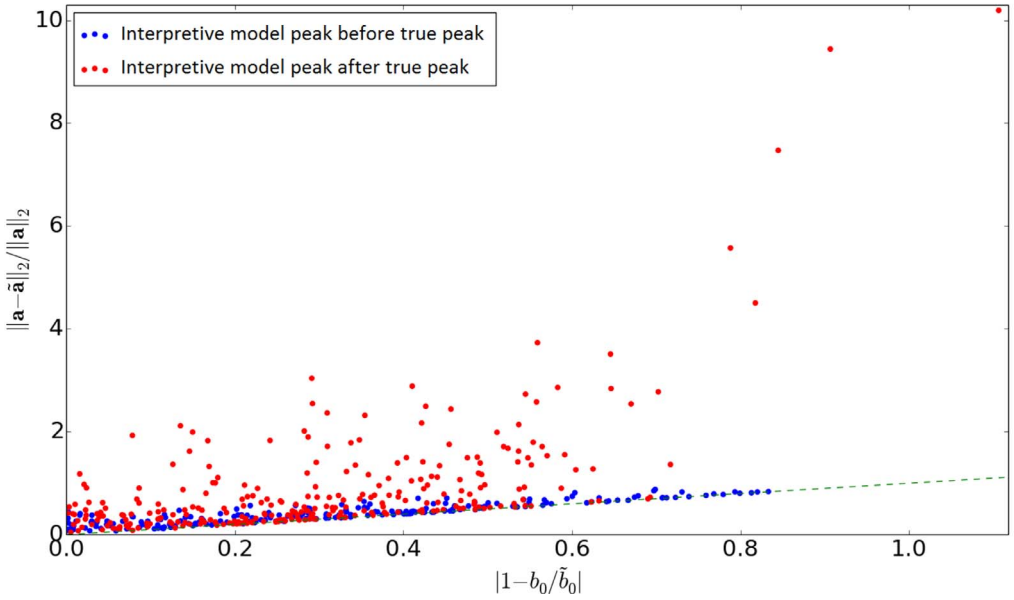

Fig. 4. Top: empirical pdf of normalized L^2 estimation error of $h(x = 0, y, t)$ from the ensemble of 500 realizations. Bottom: scatter plot of relative estimation error against lower error bound.

numerical solution is evaluated using the FEniCS Logg et al., 2012) package to discretize Eqs. (32–33), using finite element methods in space and an implicit Euler method in time. Simulated hydraulic head data is recorded at the point (4, 2) for each realization of $K(\boldsymbol{x})$ (Fig. 2), and the 50-term LEM is used along with $T = 100$ $[T]$ to reconstruct the time series of hydraulic head values on the left boundary (Fig. 3). The same procedure is followed to generate the interpretive model, $\tilde{b}(t)$ except $K(\boldsymbol{x}) = 1$ for all $\boldsymbol{x}$ (i.e., $Y(\boldsymbol{x}) = 0$ for all $\boldsymbol{x}$) is employed.

3.2. Discussion of results

Given that the random hydraulic conductivity fields chosen for the forward modeling were only moderately heterogeneous, and that choice of a spatially uniform interpretive model is a natural response to unresolved heterogeneity, the wide array of possible reconstructions is notable. In particular, a bifurcation of the response classes was noted based on whether the peaks of the forward model impulse response, b, preceded or lagged that of the interpretive model, $\tilde{b}$. In cases in which the interpretive model predicted a faster response than existed in reality, the reconstruction of the decaying exponential boundary condition was typically smooth, with its peak at a time significantly greater than zero: the delayed reconstruction of the boundary condition compensated for the over-rapid model. However, because signal causality is enforced, the model cannot respond to an earlier-than-anticipated arrival with a non-zero signal at negative time. Instead, the optimal reconstruction features a large peak at time zero, followed by decaying corrective oscillations. This bifurcation of behavior is potentially useful as a model diagnostic tool that does not require any a priori knowledge of the true model (other than that it possesses a unimodal structure): multiple candidate interpretive models could be tested with peaks at different locations, and the true peak location pinpointed by the disappearance of the spurious oscillations.

In Fig. 4 (top), the empirical pdf for the L^2 error, normalized by the L^2 norm of the signal being reconstructed, is shown. It is apparent that even for moderate heterogeneity, reconstruction error on the same magnitude as the signal itself is to be expected. In Fig. 4 (bottom), the

L^2 error of approximation in the reconstruction of the boundary condition for each of the 500 realizations is plotted against the zero-order lower error bound in Eq. (16).

4. Summary and conclusion

Systematic model error was considered in the context of inverse problems in systems whose output signal is determined by convolution of an input signal with a transfer function, or impulse response, which describes system behavior. Using a generalized Fourier series expansion in Laguerre basis functions, it was possible to translate the signal reconstruction inverse problem into a matrix inverse problem whose structure may be analyzed using some classic, and some apparently new, results in matrix algebra. It is thus seen possible to place upper and lower bounds on the L^2 signal reconstruction error as in terms of the transfer function infidelity. It was also observed that the use of additional measurement locations is not expected to improve reconstruction performance in the face of model error.

The inverse problem of recovering river level history from remote measurements at a well, which has a convolution structure, was chosen for Monte Carlo study. Forward predictions were generated by solving the groundwater flow equation on a mildly heterogeneous hydraulic conductivity field, and these were interpreted using the groundwater flow equation, assuming a homogeneous hydraulic conductivity field. The L^2 reconstruction error, ϵ, for the river level was established for all realizations, and this error was compared with the error bound developed above. The simple lower bound derived here Eq. (16) was found to be informative regarding the reconstruction error in the specific realizations. A qualitative bifurcation in the reconstructed signal was discovered, depending on the location of the peak of the interpretation model transfer function relative to that of the true model. Looking forward, this may prove to be a useful tool for transfer function identification.

The Laguerre expansion approach, because of its high degree of structure, relative simplicity and computational efficiency, may also prove to be a profitable foundation for further analysis of model error. The matrix transformation of the inverse problem developed here can be also applied for other problems of interest such as groundwater contaminant transport, propagation of low-frequency seismic waves, heat flow, infectious disease transmission, population dynamics, spreading chemical/biochemical substances in atmosphere, and many others.

Acknowledgements

The authors acknowledge the support of the LANL Environmental Programs. All data is synthetic; the authors maintain an archive of codes and simulation output employed in the paper.

Appendix A. Two results on triangular Toeplitz matrix manipulation

Here, we establish two apparently original results: that the inverse of a (lower or upper) triangular Toeplitz matrix is itself a (lower or upper) triangular Toeplitz matrix, and that the product of two (both lower or both upper) triangular Toeplitz matrices is similarly a (lower or upper) triangular Toeplitz matrix. Without loss of generality, we assume the matrices are lower triangular Toeplitz (LTT) in both proofs.

Lemma 1 (*Inversion of triangular Toeplitz matrices*). *If* $\mathbf{M}$ *is a triangular Topelitz matrix, then* $\mathbf{M^{-1}}$ *is also triangular Topelitz.*

Proof. Let $\mathbf{M_N}$ be an $N \times N$ LTT matrix, N arbitrary, and let $\mathbf{M_N^{-1}}$ be its inverse. It may be shown by induction that $\mathbf{M_N^{-1}}$ is LTT. This argument makes repeated use of the following identity for block-triangular matrices (Bernstein, 2005, p. 71):

$$\begin{bmatrix} A & 0 \\ C & D \end{bmatrix}^{-1} = \begin{bmatrix} A^{-1} & 0 \\ -D^{-1}CA^{-1} & D^{-1} \end{bmatrix}, \tag{A.1}$$

where A, 0, C, and D are compatibly-shaped sub-matrices.

The base case is trivial: note that that for any 2×2 LTT matrix, $\mathbf{M_2}$, Eq. (A.1) implies directly that $\mathbf{M_2^{-1}}$ is LTT.

For the inductive step, assume that it has been established for $(N-1) \times (N-1)$ LTT matrices that their inverses are LTT. Define $\mathbf{M_{N-1}}$ to be the sub-matrix consisting of the first $N-1$ rows and first $N-1$ columns of an arbitrary LTT matrix, $\mathbf{M_N}$. Note that $\mathbf{M_{N-1}}$ is also LTT, and by our inductive assumption so is $\mathbf{M_{N-1}^{-1}}$. It is valid to apply Eq. (A.1) in two different ways. First, make the assignment $A \equiv \mathbf{M_{N-1}}$ and apply Eq. (A.1). This implies that A^{-1} is LTT, and also that $\mathbf{M_N^{-1}}$ is lower triangular. This analysis has accounted for all but the N-th row of $\mathbf{M_N^{-1}}$. To see that the constant descending diagonals continue into the bottom row, note that the sub-matrix consisting of the last $N-1$ rows and last $N-1$ columns of $\mathbf{M_N}$ is also $\mathbf{M_{N-1}}$. Make the assignment $D \equiv \mathbf{M_{N-1}}$ and apply Eq. (A.1) again, implying that D^{-1} is LTT, and also that $A^{-1} = D^{-1}$ (Note that these are both $(N-1) \times (N-1)$ matrices which are largely overlapping, and do not participate in the same block partitioning of $\mathbf{M_N^{-1}}$). It is thus shown that all descending diagonals of $\mathbf{M_N^{-1}}$ are constant (the single element $(\mathbf{M_N^{-1}})_{N1}$ can have any value without affecting this). It has thus been shown that, subject to our inductive assumption, $\mathbf{M_N^{-1}}$ is LTT for arbitrary LTT $\mathbf{M_N}$.

By combination of base case and inductive step it follows that if $\mathbf{M_N}$ is an LTT $N \times N$ matrix then so is $\mathbf{M_N^{-1}}$, $\forall N \geq 2$. □

Lemma 2 (*Multiplication of triangular Toeplitz matrices*). *If* $\mathbf{F}$ *and* $\mathbf{G}$ *are triangular Topelitz matrices with the same dimensions, then* $\mathbf{FG}$ *is a triangular Topelitz matrix.*

Proof. For any two $N \times N$ matrices $\mathbf{F}$ and $\mathbf{G}$, it is true that the element $(\mathbf{FG})_{ij} = \sum_{k=1}^{N} \mathbf{F}_{ik}\mathbf{G}_{kj}$. If the matrices are also LTT, it follows that

$$\mathbf{F}_{ik} = \begin{cases} 0 & i < k \\ \mathbf{f}_{i-k} & i \leq k \end{cases} \tag{A.2}$$

$$\mathbf{G}_{kj} = \begin{cases} 0 & k < j \\ \mathbf{g}_{k-j} & k \geq j \end{cases}, \tag{A.3}$$

where $\mathbf{f}_n$ and $\mathbf{g}_n$ are the elements on the n-th (sub-)diagonal of $\mathbf{F}$ and $\mathbf{G}$, respectively (with the main diagonal having index 0, the first sub-diagonal having index 1, and so on). Then it follows that

$$(\mathbf{FG})_{ij} = \sum_{k=j}^{i} \mathbf{f}_{i-k}\mathbf{g}_{k-j} \tag{A.4}$$

$$= \sum_{k=0}^{i-j} \mathbf{f}_{(i-j)-k}\mathbf{g}_k. \tag{A.5}$$

$(\mathbf{FG})_{ij}$ is thus a function only of $i-j$ and is zero for $i<j$. Thus, $\mathbf{FG}$ is LTT. □

References

Abate, J., Choudhury, G.L., Whitt, W., 1996. On the Laguerre method for numerically inverting laplace transforms. INFORMS J. Comput. 8 (4), 413–427. http://dx.doi.org/10.1287/ijoc.8.4.413. ISSN 1091–9856

Bernstein, D.S., 2005. Matrix Mathematics. Princeton University Press, Princeton, NJ.

Beven, K., Binley, A., 1992. The future of distibuted models: model calibration and uncertainty prediction. Hydrol. Process. 6, 279–298. http://dx.doi.org/10.1002/hyp.3360060305. ISSN 0885-6087

Brynjarsdóttir, J., O'Hagan, A., 2014. Learning about physical parameters: the importance of model discrepancy. Inverse Probl. 30 (11), 114007. http://dx.doi.org/10.1088/0266-5611/30/11/114007. ISSN 0266–5611

Bui-Thanh, T., 2012. A Gentle Tutorial on Statistical Inversion using the Bayesian Paradigm. ICES Report 12–18. Technical report. University of Texas at Austin, Austin, TX.

Churchill, R.V., 1963. Fourier Series and Boundary Value Problems. McGraw-Hill, New York.

Del Giudice, D., Löwe, R., Madsen, H., Mikkelsen, P.S., Rieckermann, J., 2015. Comparison of two stochastic techniques for reliable urban runoff prediction by modeling systematic errors. Water Resour. Res. 51 (7), 5004–5022. http://dx.doi.org/10.1002/2014WR016678. ISSN 1944-7973

Doherty, J., Welter, D., 2010. A short exploration of structural noise. Water Resour. Res. 46 (5), 1–14. http://dx.doi.org/10.1029/2009WR008377. ISSN 0043-1397

Gaganis, P., Smith, L., 2001. A Bayesian approach to the quantification of the effect of model error on the predictions of groundwater models. Water Resour. Res. 37 (9), 2309–2322. http://dx.doi.org/10.1029/2000WR000001. ISSN 1944-7973

Gong, W., Gupta, H.V., Yang, D., Sricharan, K., Hero, A.O., 2013. Estimating epistemic and aleatory uncertainties during hydrologic modeling: an information theoretic approach. Water Resour. Res. 49 (4), 2253–2273. http://dx.doi.org/10.1002/wrcr.20161. ISSN 0043-1397

Gupta, H.V., Clark, M.P., Vrugt, J.A., Abramowitz, G., Ye, M., 2012. Towards a comprehensive assessment of model structural adequacy. Water Resour. Res. 48 (8), 1–16. http://dx.doi.org/10.1029/2011WR011044. ISSN 0043-1397

Gupta, H.V., Wagener, T., Liu, Y., 2008. Reconciling theory with observations: elements of a diagnostic approach to model evaluations. Hydrol. Process. 22 (18). http://dx.doi.org/10.1002/hyp.6989. ISSN 0885-6087

Hansen, P.C., 1992. Analysis of discrete ill-posed problems. SIAM Rev. 34 (4), 561–580. http://dx.doi.org/10.1137/1034115. ISSN 0036-1445

Hansen, S.K., Kueper, B.H., 2009. An efficient method for asymptotic solution to some linear PDEs having arbitrary time-varying type I boundary conditions. Appl. Math. Comput. 207 (1), 273–278. http://dx.doi.org/10.1016/j.amc.2008.10.008. ISSN 0096-3003

Hansen, S.K., Vesselinov, V.V., 2016. Contaminant point source localization error estimates as functions of data quantity and model quality. J. Contam. Hydrol. 193, 74–85. http://dx.doi.org/10.1016/j.jconhyd.2016.09.003. ISSN 0169-7722

Kashyap, R.L., 1982. Optimal choice of AR and MA parts in autoregressive moving average models. IEEE Transactions on Pattern Analysis and Machine Intelligence, PAMI-4 (2), 99–104. http://dx.doi.org/10.1109/TPAMI.1982.4767213. ISSN 0162–8828

Kennedy, M.C., O'Hagan, A., 2001. Bayesian calibration of computer models. J. R. Stat. Soc. 63 (3), 425–464. http://dx.doi.org/10.1111/1467-9868.00294. ISSN 1369–7412

Krzysztofowicz, R., 1999. Bayesian theory of probabilistic forecasting via deterministic hydrologic model. Water Resour. Res. 35 (9), 2739–2750. http://dx.doi.org/10.1029/1999WR900099. ISSN 1944-7973

Lin, Z., Beck, M.B., 2012. Accounting for structural error and uncertainty in a model: an approach based on model parameters as stochastic processes. Environ. Modell. Software 27–28, 97–111. http://dx.doi.org/10.1016/j.envsoft.2011.08.015. ISSN 1364-8152

Logg, A., Mardal, K.-A., Wells, G., 2012. Automated solution of differential equations by the finite element method: The FEniCS book. Springer, Berlin. http://dx.doi.org/10.1007/978-3-642-23099-8.

Montanari, A., 2007. What do we mean by 'uncertainty'? the need for a consistent wording about uncertainty assessment in hydrology. Hydrol. Process. 21 (6), 841–845. http://dx.doi.org/10.1002/hyp.6623. ISSN 0885-6087

Refsgaard, J.C., van der Sluijs, J.P., Brown, J., van der Keur, P., 2006. A framework for dealing with uncertainty due to model structure error. Adv. Water Resour. 29 (11), 1586–1597. http://dx.doi.org/10.1016/j.advwatres.2005.11.013. ISSN 0309-1708

Renard, B., Kavetski, D., Kuczera, G., Thyer, M., Franks, S.W., 2010. Understanding predictive uncertainty in hydrologic modeling: the challenge of identifying input and structural errors. Water Resour. Res. 46 (5), 1–22. http://dx.doi.org/10.1029/2009WR008328. ISSN 0043-1397

Schwarz, G., 1978. Estimating the dimension of a model. Ann. Stat. 6 (2), 461–464. http://dx.doi.org/10.1214/aos/1176344136. ISSN 0090–5364

Sneider, R., Trampert, J., 1999. Inverse Problems in Geophysics. In: Wirgin, A. (Ed.), Wavefield Inversion. Springer-Verlag, Wien, pp. 119–190. http://dx.doi.org/10.1007/978-3-7091-2486-4.

Vrugt, J.A., Braak, C.J.F.t., Clark, M.P., Hyman, J.M., Robinson, B.A., 2008. Treatment of input uncertainty in hydrologic modeling: doing hydrology backward with Markov chain Monte Carlo simulation. Water Resour. Res. 44 (12), 1–52. http://dx.doi.org/10.1029/2007WR006720. ISSN 0043–1397

Vrugt, J.A., Sadegh, M., 2013. Toward diagnostic model calibration and evaluation: approximate bayesian computation. Water Resour. Res. 49 (7), 4335–4345. http://dx.doi.org/10.1002/wrcr.20354. ISSN 0043-1397

White, J.T., Doherty, J.E., Hughes, J.D., 2014. Quantifying the predictive consequences of model error with linear subspace analysis. Water Resour. Res. 50 (2), 1152–1173. http://dx.doi.org/10.1002/2013WR014767. ISSN 1944-7973

Xu, T., Valocchi, A.J., 2015. A Bayesian approach to improved calibration and prediction of groundwater models with structural error. Water Resour. Res. 51 (11), 9290–9311. http://dx.doi.org/10.1002/2015WR017912. ISSN 1944-7973

Zhang, D., Lu, Z., 2004. An efficient, high-order perturbation approach for flow in random porous media via Karhunen–Loeve and polynomial expansions. J. Comput. Phys. 194 (2), 773–794. http://dx.doi.org/10.1016/j.jcp.2003.09.015. ISSN 0021-9991